HENRY GRANJON PRIZE COMPETITION 2005
Winner, Category B
"Materials behaviour and weldability"

MICROSTRUCTURE AND PROPERTIES OF NOVEL HIGH STRENGTH STEEL WELD METALS

E. Keehan
Department of Experimental Physics, Chalmers University of Technology (Sweden)

ABSTRACT

The relationship between alloying content, microstructure and properties has been studied for high strength steel weld metals with 7 wt. % nickel. Following neural network predictions, shielded metal arc welding was used to produce experimental welds with manganese at 0.5 or 2 wt. %, while carbon was varied between 0.03 and 0.11 wt. %. High manganese was positive for strength but very negative for impact toughness while manganese reductions lead to large impact toughness increases. Carbon additions up to 0.11 wt. % were found to increase yield strength to over 900 MPa while impact toughness was maintained and over 60 J was recorded at –100 °C. High resolution microscopy was used to characterise the microstructure. In dendrite core regions a mixture developed of predominantly upper bainite and a coarse grained, previously not documented constituent, characterised to be coalesced bainite. In inter-dendritic regions mainly martensite formed for high manganese weld metals. Manganese reductions were found to promote upper bainite while carbon additions were found to promote martensite. A constitutional diagram was constructed that summarises microstructure as a function of manganese and nickel contents. Mechanical properties of the weld metals were rationalised in terms of the relative amounts of the different microstructural constituents.

IIW-Thesaurus keywords: *Weld metal; MMA welding; Arc welding; Yield strength; Mechanical properties; Strength; Ultimate tensile strength; Impact toughness; Toughness; Microstructure; Austenite; Bainite; Martensite; Neural networks; Artificial intelligence; Mathematical models; High strength steels; Steels; Reference lists.*

1 BACKGROUND

Steels with yield strengths in the region of 1 000 MPa that possess good impact toughness have been readily available for some time. They are increasingly employed in many applications offering both size and weight reduction. In many applications, it is an engineering requirement that a weld metal with matching or overmatching strength is used in the joining. It is well known that maintaining good toughness becomes more problematic as strength levels increase above the region of 690 MPa (100 ksi) with more flexible and productive flux shielded welding methods such as shielded metal arc welding (SMAW) [1, 2]. As a result there is a need to develop new high strength welding consumables that meet the market requirements.

To date, high strength steel weld metals have usually C less than 0.2 wt. %, Ni less than 4 wt. % and Mn less than 3 wt. % [1, 3-18]. Results generated yield strengths ranging from below 500 MPa to above 1 000 MPa. However, with the common flux shielded welding processes, good impact toughness was mostly achieved at lower yield strengths. Promising work with SMAW carried out by Lord [10] used the composition of a commercial SMAW consumable with 3 Ni, 2 Mn, 0.5 Cr, 0.6 Mo, 0.05 C as the basis of development. He increased nickel concentrations to 4 wt. % and decreased Mn levels to 0.8 wt. %. It was found that impact toughness increased to 74 J at – 60 °C and the yield strength was reduced to 809 MPa [10]. Kang followed the trend of increasing Ni and reducing Mn with metal cored wires recording an impact toughness of 55 J at – 60 °C with Ni at 6.95 wt. % and Mn at 0.52 wt. %. Tensile strength of 684 MPa was predicted for this alloy from hardness results. From microstructural investigations, the presence of lath martensite and various forms of ferrite was reported [19]. From literature it is generally found that as impact toughness increases, yield and tensile strength decrease. To limit strength losses, carbon additions and reducing interpass temperature have been most effective [20-21]. For example carbon levels up to 0.08 wt. % combined with 2-4 Ni and 1.4-2.0 Mn were found good for strength with limited losses in impact toughness [20]. In another study it was found that yield and ultimate tensile strength also increased with decrease in interpass temperature [21]. In both

Doc. IIW-1703-05 (ex-doc. IX-2146-05) recommended for publication by Commission IX "Behaviour of metals subjected to welding".

cases, changes in mechanical properties were claimed to be strongly related to the microstructure described as mixtures of martensite and bainite.

In work presented elsewhere [22], neural network modelling was engaged to optimise the development process and to allow the effects of a wide variety of parameters to be perceived quickly. The technique and the advantages it offers materials science are further described in [23-25]. In particular, the models predicted that manganese reductions from 2 to 0.5 wt. % at 7 wt. % nickel lead to large increases in impact toughness. Setting Ni and Mn at 7 and 0.5 wt % respectively, further predictions suggested that carbon additions would increase strength significantly. It was also suggested that impact toughness levels at – 60 °C were to remain acceptable with carbon additions up to at least the region of 0.12 wt. %.

This paper is an overview of a larger study [26] investigating the effects of changing C, Mn and Ni contents on the microstructure and the mechanical properties of high nickel high strength steel weld metals. Selected results are presented here and more details along with comprehensive discussion may be found elsewhere [22, 26-31].

2 EXPERIMENTAL TECHNIQUES

Five experimental weld metals were produced using SMAW to study the changes in mechanical and microstructural behaviour for Mn concentrations of 0.5 or 2.0 wt. %, and carbon additions from 0.03 to 0.11 wt. % with Ni at 7 wt. %.

Welded joints were made according to ISO 2560 using 20 mm plates with a backing plate. The joints were buttered prior to the deposition of the experimental weld metals that took place in 33 cm runs with two or three runs per layer. The energy input and interpass temperature are presented in Table 1. Names were assigned to the weld metals according to composition and interpass temperature. 7 is the Ni content, 2 or 0.5 is the Mn content, L, M or H are the low, medium, or high carbon contents and 200 or 250 is the maximum interpass temperature. The estimated cooling time between 800 and 500 °C ($t_{8/5}$) was calculated using the WeldCalc program [32]. Samples of weld metal were analysed using optical emission spectrometry and Leco combustion equipment. The compositions of the weld metals are presented in Table 1.

Charpy impact testing and tensile testing were performed in compliance with standard EN 10045-1. For Charpy testing, transverse specimens were machined having dimensions $55 \times 10 \times 10$ mm. These were then notched perpendicular to the welding direction in the weld metal centre and 2 or 3 specimens were tested at each temperature. Tensile specimens were machined longitudinally from the centre of the weld deposits with a specimen diameter of 10 mm and a gauge length of 70 mm.

Specimens from the weld metal cross section, extracted perpendicular to the welding direction were mounted in bakelite, wet ground, polished to 1 μm diamond paste and etched using 2 % nital etchant for analysis with light optical microscopy (LOM) and field emission gun scanning electron microscopy (FEGSEM). A Leitz Aristomet light optical microscope and a Leo Ultra 55 FEGSEM were used in these examinations. Polished specimens were examined with scanning electron microscopy (SEM) in the back scattered mode and elemental analysis was carried out using Energy Dispersive X-ray analy-

Table 1 – Welding parameters and chemical composition

Weld Metal	7-2L250	7-0.5L250	7-0.5L200	7-0.5M200	7-0.5H200
Welding parameters					
Energy input, E (kJ mm^{-1})	1.2	1.0	1.3	1.4	1.3
Interpass temperature, IPT (°C)	250	250	200	200	200
Estimated cooling time between 800 and 500 °C, calculated from WeldCalc [32], $t_{8/5}$ (s)	12	10	10	11	10
Composition in wt. %, unless otherwise stated					
C*	0.032	0.024	0.030	0.061	0.110
Mn	2.02	0.64	0.61	0.56	0.53
Ni	7.23	6.60	6.11	6.84	7.04
Cr	0.47	0.21	0.16	0.15	0.14
Si	0.25	0.35	0.40	0.34	0.38
S*	0.008	0.008	0.009	0.006	0.007
P	0.011	0.012	0.010	0.011	0.008
Mo	0.63	0.40	0.38	0.35	0.40
V	n.a.	n.a.	0.018	0.014	0.016
Cu	0.03	0.03	0.02	0.01	n.a.
O / ppm*	380	400	340	350	260
N / ppm*	250	197	150	160	100

* indicates elements analysed using Leco combustion equipment.
"n.a." are elements not analysed.

sis (EDX). For TEM studies, 3 mm disc shape samples, perpendicular to the welding direction, were ground to between 50 and 80 μm in thickness and then jet electropolished at – 35 °C using 10 % perchloric acid in methanol. After electropolishing the specimens were further thinned by ion beam milling for a few minutes at a low angle using a Gatan Precision Ion Polishing System (PIPS). These specimens were examined with a Jeol 2000 FX or a Philips CM200 TEM.

Dilatometer specimens in the form of cylinders with a diameter of 3 mm and a length of 10 mm were machined from the centre of the welded joint. These were then investigated using a Theta Dilatronic III dilatometer. The specimens were heated to 1 000 °C at a rate of 25 °C/s, held for 5 minutes and afterwards cooled to room temperature at different cooling rates. Individual samples were used for each cooling rate.

3 RESULTS

3.1 Strength and impact toughness

The results of tensile testing and Charpy impact toughness testing at 22, – 40, – 100 °C are presented in Table 2. Comparing 7-2L250 with 7-0.5L250, a large decrease in ultimate tensile strength (UTS) and increase in impact toughness was measured as a result of reducing Mn content. It is seen that 7-2L250 had relatively low impact toughness but good yield strength (YS), 795 MPa, and high UTS (over 1 000 MPa). Weld metal 7-0.5L250, with the best impact toughness both at room temperature and at – 40 °C, recorded lower strength with UTS at 823 MPa and YS at 721 MPa.

Interpass temperature was reduced to 200 °C in order to promote faster cooling with the aim of increasing strength. Comparing 7-0.5L250 with 7-0.5L200 that have similar compositions, yield strength increased from 721 MPa to 777 MPa. However this trend was limited with UTS which only increased from 823 MPa to 831 MPa. The impact toughness, was maintained very well with over 100 J recorded at – 40 °C.

The effect of carbon additions on mechanical properties were then examined with the deposition of 7-0.5M200 and 7-0.5H200. From Table 2, it is seen that carbon additions increased both YS and UTS. 7-0.5H200 recorded the best YS of all alloys studied with 912 MPa achieved at a carbon level of 0.11 wt. %. Given the strength, high impact toughness was also recorded with average 63 J at – 100 °C.

3.2 Microstructure – The last bead

The last bead of each weld was found to consist of a columnar structure with the columns varying in size but normally these were less than 0.5 mm in width. The columns were further subdivided into a cellular structure of dendrites with a thickness between 10 and 30 μm (see Figure 1).

Figure 2 presents LOM micrographs showing the variation of microstructure in the as-deposited last bead as a result of changing manganese and carbon content. The former dendrite boundaries can be seen clearly more or less in all images. The microstructure is very fine scale, typical of martensite or bainite, but it is not possible to discriminate between the two with LOM due to their similar morphologies. Large grains not commonly found in high strength steel weld metals were also observed in particular with 7-2L250. The progressive effect of changing carbon from 0.03 to 0.11 wt. % can be observed by comparing micrographs from 7-0.5L200, 7-0.5M200 and 7-0.5H200. It is found that some larger grains appear in the 7-0.5M200, but apart from these, generally the microstructure becomes very fine with increase of carbon content. It is not possible with LOM to identify the microstructure with full certainty and inves-

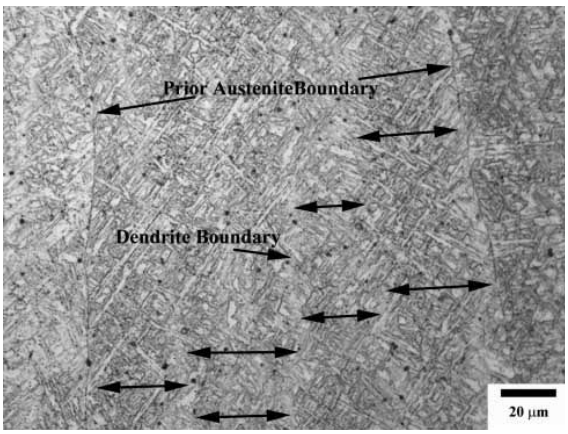

The dendrites that formed within the columnar structure as the weld metal solidified are seen.

Figure 1 – LOM micrograph from 7-0.5L200 showing a fine scale microstructure

Table 2 – Yield strength (YS), ultimate tensile strength (UTS) and Charpy impact toughness for the experimental weld metals

Weld Metal	7-2L250	7-0.5L250	7-0.5L200	7-0.5M200	7-0.5H200
YS	795	721	777	858	912
UTS	1 006	823	831	895	971
Impact toughness (J)					
22 °C	45	124	123	109	85
– 40 °C	32	112	101	90	78
– 100 °C	n.m.	55	60	79	63

"n.m." stands not measured.

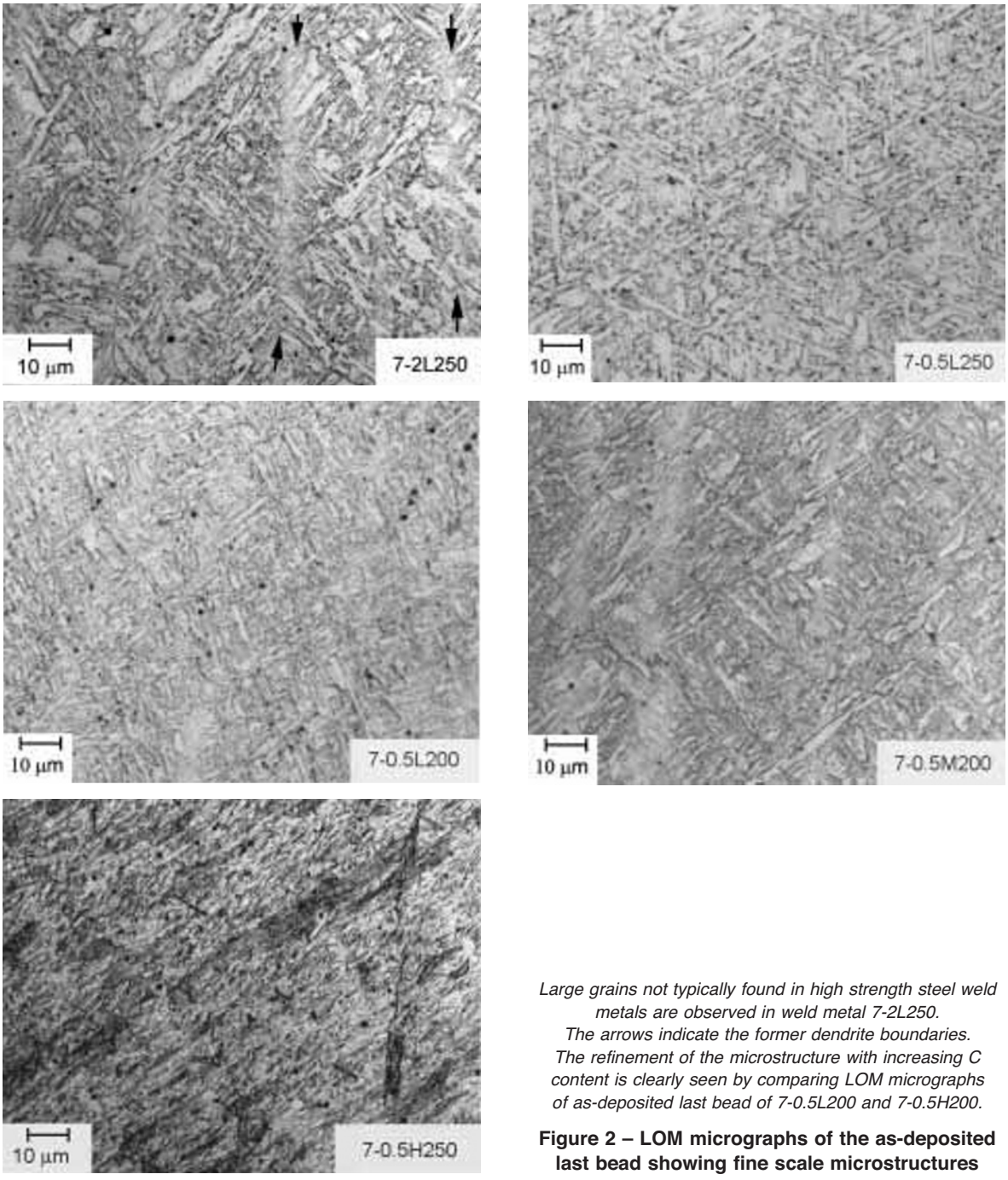

Large grains not typically found in high strength steel weld metals are observed in weld metal 7-2L250. The arrows indicate the former dendrite boundaries. The refinement of the microstructure with increasing C content is clearly seen by comparing LOM micrographs of as-deposited last bead of 7-0.5L200 and 7-0.5H200.

Figure 2 – LOM micrographs of the as-deposited last bead showing fine scale microstructures

tigations with instruments offering better resolution are necessary. This work has been carried out and full details may be found elsewhere [22, 28-31]. A summary is presented here.

The microstructure of the as-deposited last bead in weld metals 7-2L250 and 7-0.5L250 is shown in Figure 3. Focusing on weld metal 7-2L250, it was investigated in great detail both with FEGSEM and TEM. The constituent with a large grain size, also seen with LOM in Figure 2, was characterised to be a previously not reported variant of bainite that forms through a coalescence of bainitic ferrite plates when martensite start temperature (M_s) and bainite start temperature (B_s) are close. Full details of its characterisation are presented elsewhere [28]. A FEGSEM micrograph showing coalesced bainite at slightly higher magnification is presented in Figure 4. It was found that the coalesced bainite develops without the typical bainite subunit structure of platelets with cementite at boundaries. Using electron diffraction it was found that cementite precipitates formed within the bainitic ferrite grains (see Figure 5). Generally, the coalesced bainite was found along with upper bainite in dendrite core regions, while a lath-like microstructure of martensite was found at interdendritic

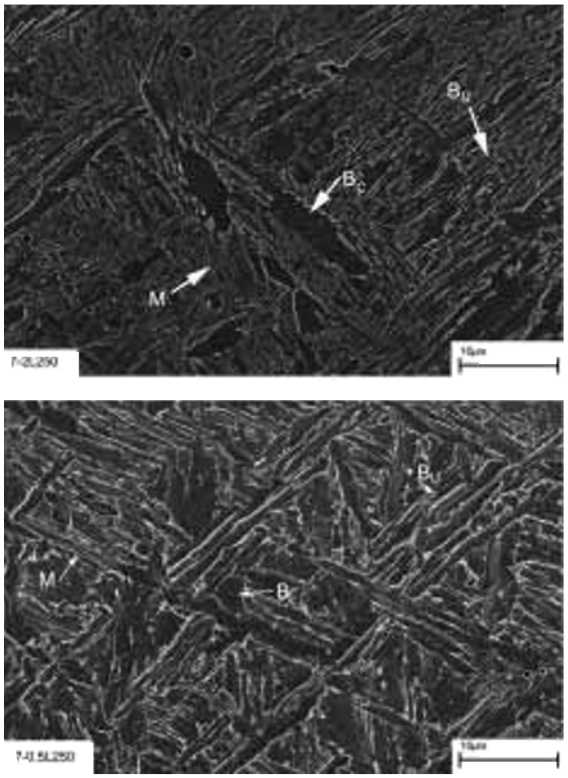

M is for martensite, B_U is upper bainite, B_L is lower bainite and B_C is coalesced bainite

Figure 3 – The microstructure in the as-deposited last bead of weld metals 7-2L250 and 7-0.5L250 imaged using FEGSEM

regions. An interdendritic region is shown at higher magnification in Figure 6 where the morphology of martensite can be seen. It is also observed that upper bainite forms a small distance away from the interdendritic region.

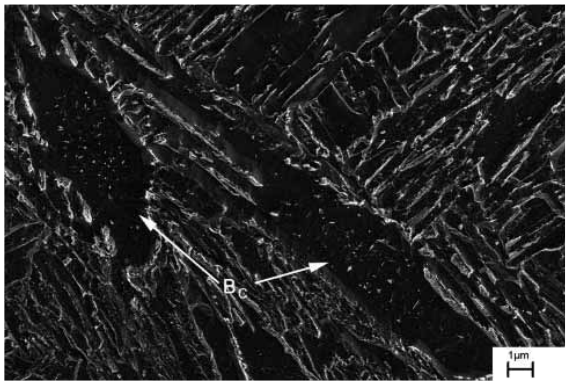

Small precipitates can be observed within the bainitic ferrite grains.

Figure 4 – Coalesced bainite in weld metal 7-2L250

Comparing the micrographs from 7-2L250 and 7-0.5L250 in Figure 3 the effects of reducing Mn content from 2 to 0.5 wt. % at nickel content of 7 wt. % may be observed. Reducing manganese gave the noticeable absence of coalesced bainite and the microstructure was found to be predominately upper and lower bainite with only small amounts of martensite present at interdendritic regions.

The effect of carbon additions on the microstructure can be observed in Figure 7. With weld metals 7-0.5L200 and 7-0.5M200 bainite was mainly found in the centre of the dendrites while a mixture of bainite and martensite developed at the prior dendrite boundary regions. Weld metal 7-0.5L200 formed the greatest amounts of upper bainite. Coalesced bainite was also observed, in particular in 7-0.5M200, but its grain size was much smaller than that observed in weld metal 7-2L250 (see Figure 3). It was found that the amount of martensite increases with increase in carbon content and with weld metal 7-0.5H250 large amounts of martensite were found within the dendrites.

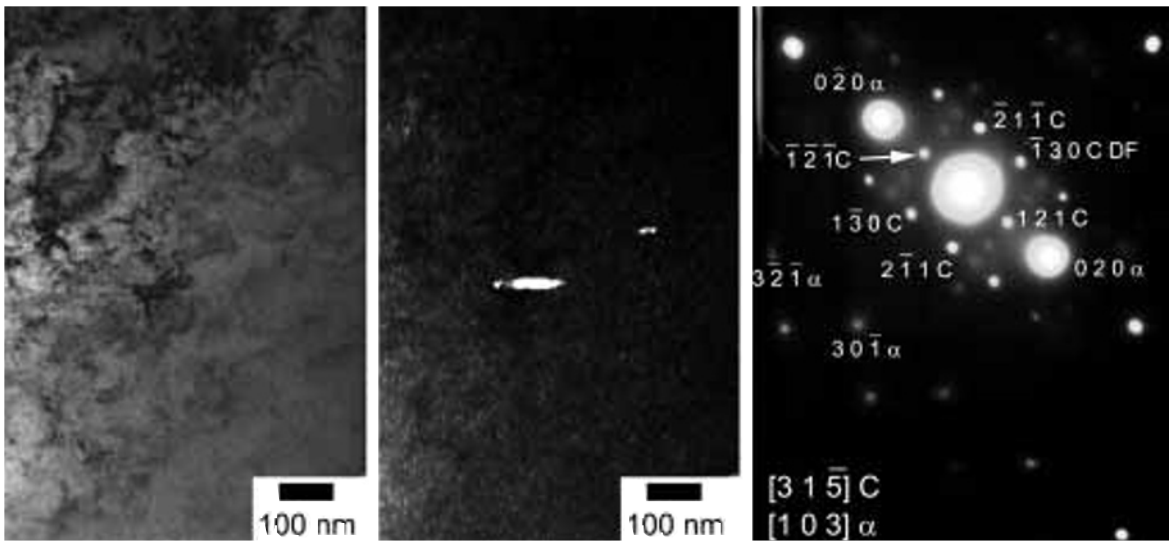

The dark field image was formed using the {–1,3,0} cementite reflection.

Figure 5 – TEM bright (left) and dark (middle) field images with corresponding diffraction pattern (right) of a cementite precipitate within a coalesced bainitic ferrite grain

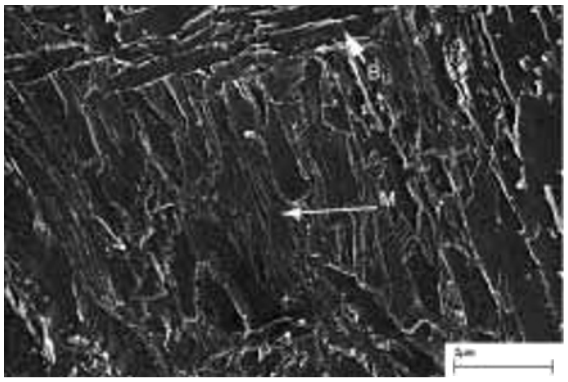

M is martensite and B_U is upper bainite.

Figure 6 – An interdendritic region in the last bead of weld metal 7-2L250 showing a mainly martensitic microstructure

3.3 Elemental segregation

When polished specimens from weld metals 7-2L250 and 7-0.5L250 were examined with SEM in the back-scattered mode, there was a clear contrast between the dendrite core regions and the interdendritic regions. This led to the observation that there may be significant elemental segregation across the former dendrites and it was decided to carry out EDX analysis. The results are presented in Table 3. In general, it was found that manganese was overestimated in all analyses. To correct for this the compositions were shifted to lower values based on the Mn content presented in Table 1 and line scans presented elsewhere [22].

3.4 Microstructure – Reheated beads

Extensive results on the microstructure of reheated regions is presented in references [22, 29-31] and only a brief summary is made here. The microstructure in central beads was as expected even more complex than the last bead which resulted from different thermal histories and tempering depending on the location within the joints. Figure 8 shows the centre of reheated beads in weld metals 7-0.5L200 and 7-0.5H200. Given the examinations in the last bead the microstructure is interpreted to be that of mainly tempered bainite with 7-0.5L200 and mainly tempered martensite with 7-0.5H200.

Table 3 – Average compositions recorded in wt. % at dendritic boundary regions and dendrite core regions in the last bead using EDX spot analysis

Weld Metal		Mn	Ni
7-2L250	Boundary	3.10 (2.50)	8.18
7-2L250	Core	2.35 (1.75)	6.30
7-0.5L250	Boundary	0.95 (0.90)	7.55
7-0.5L250	Core	0.57 (0.50)	5.83

Mn values in brackets are values adjusted using the average composition in Table 3 to allow for the overestimation of Mn with EDX.

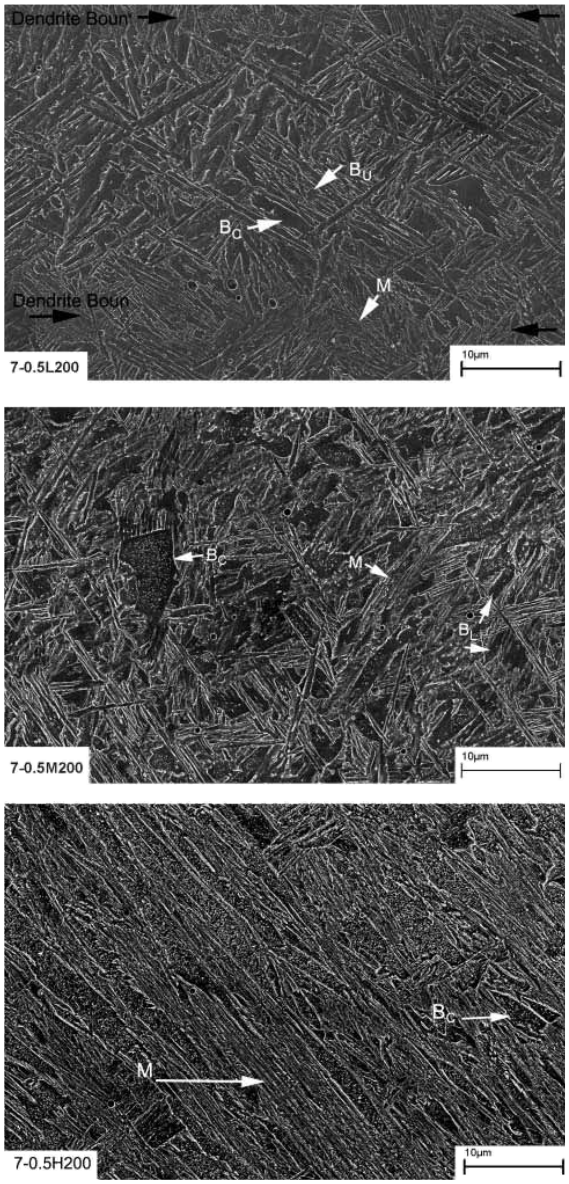

M is for martensite, B_U is upper bainite, B_L is lower bainite and B_C is coalesced bainite.

Figure 7 – The microstructure in the as-deposited last bead of weld metals 7-2L250, 7-0.5L250 and 7-0.5H200 imaged using FEGSEM

An overview of the centre in a reheated bead in weld metal 7-2L250 is shown in Figure 9. Within the micrograph, the former dendrites are clearly seen. Higher magnification FEGSEM images of 7-2L250 are presented in Figures 10 and 11. In dendrite core regions, mainly tempered bainite (see Figure 10) was seen while tempered martensite (see Figure 11) was predominantly found at interdendritic regions. In bainitic areas it was found that the carbon had redistributed within the bainitic ferrite. The cementite precipitates observed in the last bead (see Figure 4) were found to have spheroidised within the grains and coarsened at the grain boundaries. In addition very small cementite precipitates in the order of a few nanometres had formed within the bainitic fer-

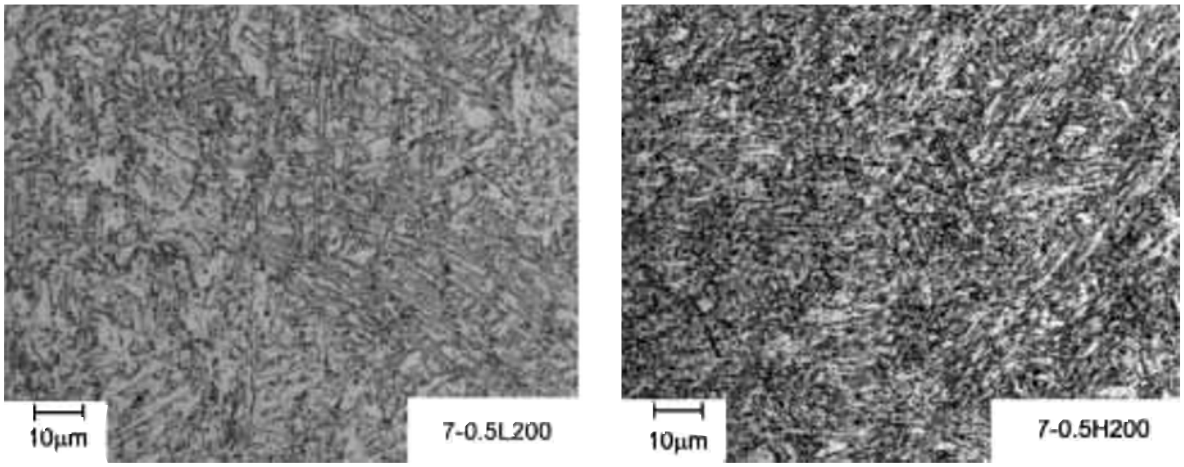

Figure 8 – LOM micrographs from 7-0.5L200 and 7-0.5H200 showing the microstructure in the bead interior of reheated central beads in the joint

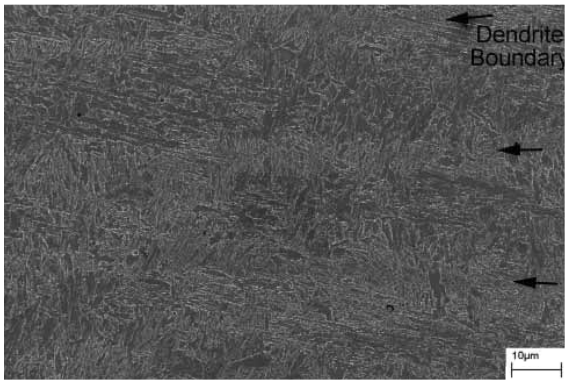

Figure 9 – A FEGSEM overview of a reheated bead in weld metal 7-2L250

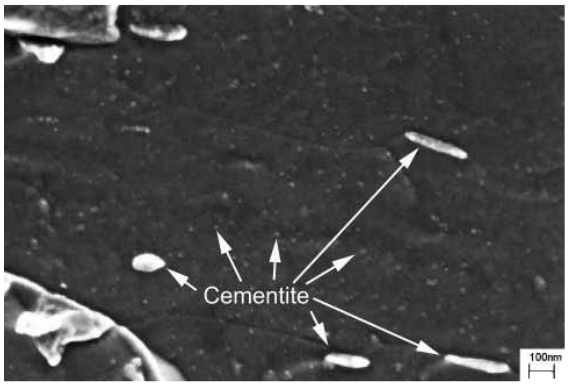

Figure 10 – A high magnification FEGSEM micrograph showing spheroidised and coarsened cementite along with newly formed small precipitates in tempered bainite in a reheated bead of weld metal 7-2L250

rite. These latter precipitates along with the former spheroidised and coarsened precipitates were confirmed to be cementite using TEM and electron diffraction [22, 31].

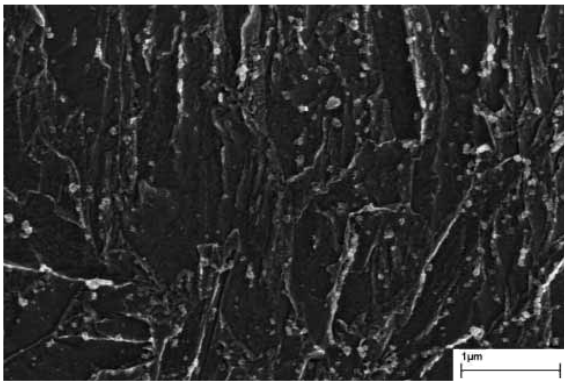

Figure 11– FEGSEM image of tempered martensite in a former interdendritic region within a reheated bead of weld metal 7-2L250

3.5 Dilatometry

Transformation temperatures for three of the weld metals are presented in Table 4. The results at cooling rates of 25-40 °C/s are representative of the cooling rates within the welded joints based on the $t_{8/5}$ calculations. Overall there was no large difference in austenite transformation temperature as a result of changing the cooling rate.

Generally, it can be said that greater nickel, manganese and carbon contents stabilise austenite to lower temperatures. Comparing 7-2L250 and 7-0.5L250 it is found that a reduction in manganese content increases both Ac_1 and Ac_3 temperatures and austenite transformation

Table 4 – Transformation temperatures recorded using dilatometry

Weld Metal	Ac_1 (°C)	Ac_3 (°C)	Transformation of γ (°C)	
			25 – 40 °C/s cooling	1 °C/s cooling
7-2L250	690	740	373	390
7-0.5L250	700	770	490	480
7-0.5H200	685	770	355	365

on cooling takes place in the region of 100 degrees higher. Carbon additions were found to reduce the Ac_1 temperature, but interestingly, Ac_3 was maintained at the same temperature as with low carbon levels. Austenite was stabilised to very low temperatures on cooling (365 °C).

3.6 Thermo-Calc calculations

Given that it is difficult to observe with microstructural studies whether the weld metals solidified as ferrite or austenite, it was decided to use Thermo-Calc [33] to predict the transformation based on alloying content. The solidification mode is of particular importance for the final chemical distribution and knowledge was necessary to have a complete understanding of the final microstructure.

Predictions from Thermo-Calc were made using the CCTSS database and are presented in Figures 12 to 14. The liquid to solid transformation as a function of nickel content and temperature for the base compositions of weld metals 7-2L250 and 7-0.5L250 are presented as isopleths in Figures 12 and 13, respectively.

It is seen from the diagrams that ferrite can form during solidification at higher nickel contents with the lower manganese content (expected limits are 4.2 and 5 wt. % for 2.0 Mn and 0.5 wt. % respectively, Figures 12 and 13). However even with 0.5 wt. % manganese, it is observed that at 7 wt. % nickel, fully austenitic solidification will take place.

Figure 14 presents Scheil simulations for 7-0.5L250. In these calculations it is assumed that no diffusion occurs in the solid state after solidification and that the liquid is fully in equilibrium. In diagram (a) the weight fraction of solid is predicted as a function of temperature. In (b) the weight fraction of manganese content as a function of the weight fraction of solid is predicted while in (c) the weight fraction of nickel content as a function of the weight fraction of solid is shown. The Scheil calculations reaffirm that a fully FCC solidification is expected.

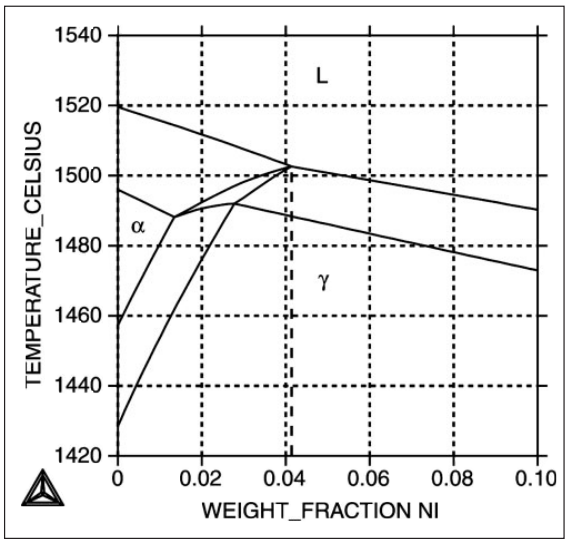

Figure 12 – Isopleth as a function of nickel content and temperature based on the composition of weld metal 7-2L250 calculated using Thermo-Calc

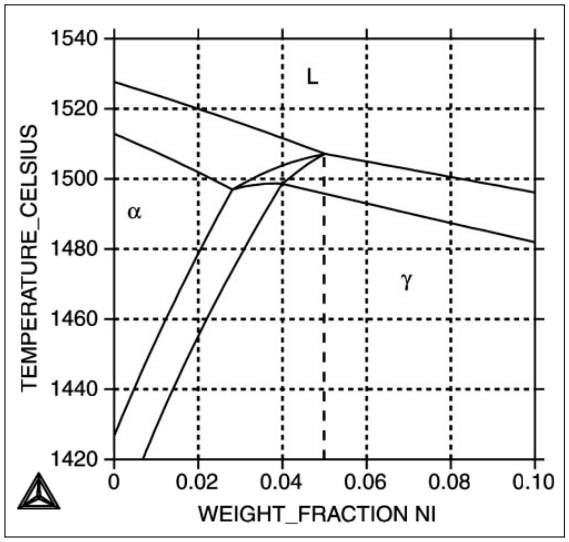

Figure 13 – Isopleth calculated with Thermo-Calc for the composition of weld metal 7-0.5L250 as a function of nickel content and temperature

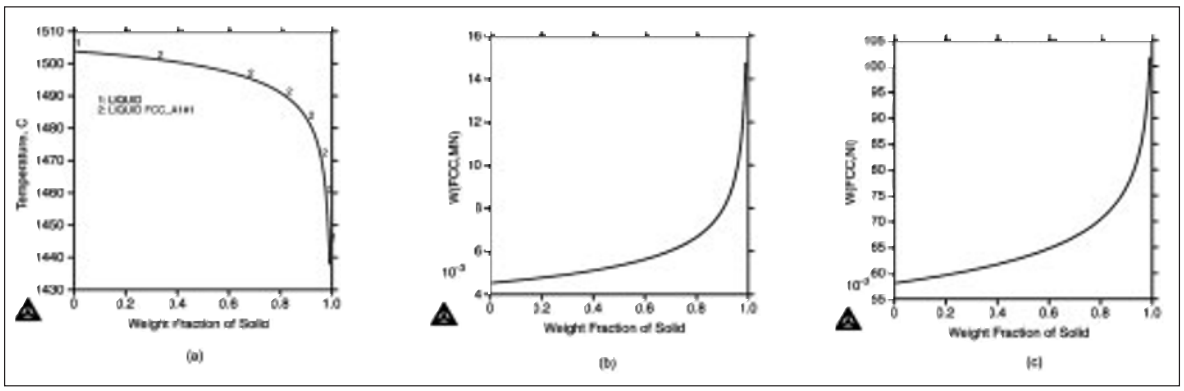

Figure 14 – Scheil simulations for weld metal 7-0.5L250 of (a) the weight fraction of solid and solidifying phase as a function of temperature, (b) manganese content as a function of the weight fraction of solid and (c) nickel content as a function of the weight fraction of solid

4 DISCUSSION

4.1 Solidification and segregation

From Thermo-Calc simulations it was suggested that all the experimental weld metals solidified completely as austenite. Diffusion of substitutional elements is much more limited in the austenitic lattice than in the ferrite lattice. The local chemistry at high temperatures is therefore inherited down to lower temperatures and thus may affect low temperature phase transformations.

An interesting comparison to make is between the Scheil simulations presented in Figure 14 and the EDX spot analysis results presented in Table 3. From the Scheil calculations for the weld metal 7-0.5L250 composition, it is predicted that the first solid to form has 0.45 wt. % Mn and 5.8 wt. % nickel (dendrite core regions) while the final composition to solidify is estimated to be 1.5 wt. % Mn and 10.2 wt. % Ni (interdendritic regions). Comparing these figures with EDX results, the average Mn and Ni content of the first solid to form was 0.57 and 5.83 wt. %, respectively, (dendrite core region) and the last solid to form had 0.95 wt. % Mn and 7.55 wt. % Ni. From this comparison, it is seen that there is a fairly good agreement between the simulations and the actual measured alloying content considering the spatial resolution of EDX analysis and the fact that some diffusion will take place. A similar agreement was found for alloy 7-2L250 supporting the conclusion that the weld metals solidified as austenite.

Given that a greater alloying content is found at interdendritic regions, phase transformations and the final microstructure will be affected. With knowledge of the effects of alloying content, the variation in microstructure both across the dendrites and between the alloys can be understood and justified as will be discussed in the following section.

4.2 Microstructural constituents

In weld metal 7-0.5L250 the microstructure was that of mainly upper and lower bainite in dendrite core regions as shown in Figure 9, with some little martensite forming at interdendritic regions. It was found that carbon additions from 0.03 to 0.11 wt. %, at 0.5 wt. % manganese and 7 wt. % nickel reduced austenite transformation temperature from 490 to 355 ^{o}C. In doing so, the microstructure became mainly martensitic (Figure 7) with some bainite also forming in dendrite core regions. Calculating the $M_s$and the B_s using the empirical equations M_s = 539 – 423 (%C) – 30.4 (%Mn) – 17.7 (%Ni) – 12.1 (%Cr) – 7.5 (%Mo) and B_s = 830 – 270 (%C) – 90 (%Mn) – 37 (%Ni) – 70 (%Cr) – 83 (%Mo) [34-35] it is seen that the predicted B_s of the low carbon weld metal of 498 ^{o}C agrees very well with the measured transformation temperature of 490 ^{o}C. For the high carbon variant, the calculated M_s is 347 ^{o}C which is also close to the measured transformation temperature of 355 ^{o}C. Clearly, predicted and measured transformation temperatures are in good agreement with the observed dominant microstructural constituents.

From dilatometry experiments, it was found that austenite transformation with weld metal 7-2L250 started in the region of 373 ^{o}C (see Table 4). The microstructure was found to be a mixture of upper bainite along with a novel constituent with a large grain size in dendrite core regions while martensite was found at interdendritic regions (see Figures 3, 4 and 6). From a detailed study [28] of the novel constituent, it was characterised to be that of coalesced bainite. Coalesced bainite is most likely to form when B_s is close to M_s (as predicted using the empirical equations) and consequently the undercooling below Ac_3 is large. The resulting transformations are then associated with large driving forces consistent with rapid nucleation and growth. When many bainitic ferrite plates are nucleated, they can coalesce into a thicker

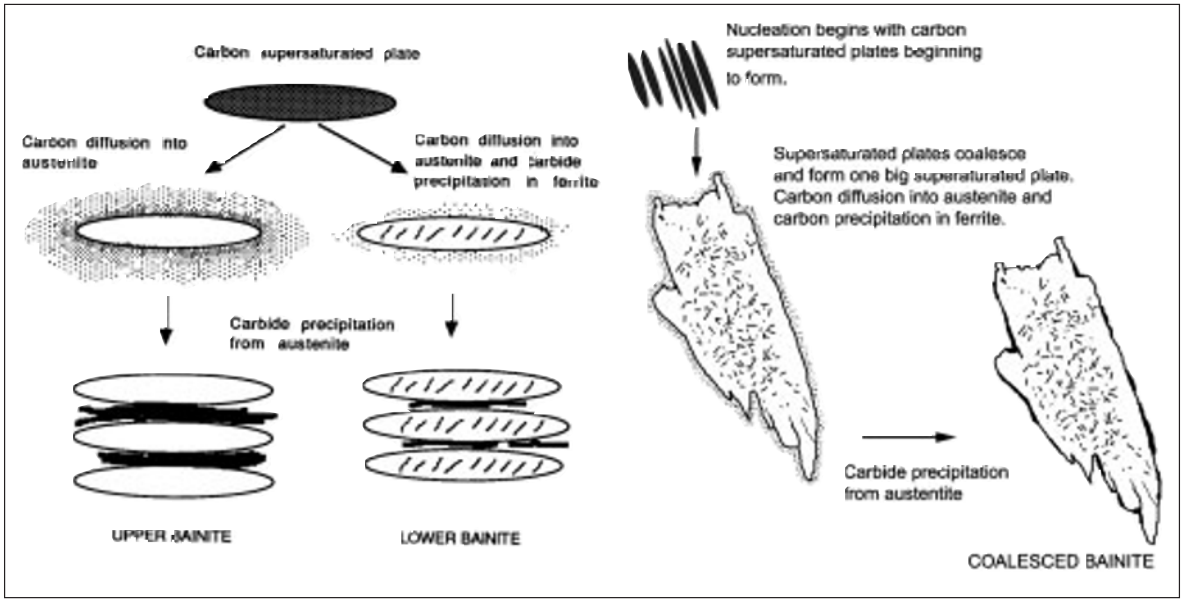

Figure 15 – Schematic representation of the formation of upper and lower bainite [36] along with coalesced bainite [28]

plate if the undercooling is large enough to sustain the strain energy [24-25]. The transformation front of coalesced bainite is found to consist of a series of finer platelets, presumably all in identical crystallographic orientation, which coalesce at some distance behind the advancing tips to generate the observed coarse grains. As temperature drops, within the centre of the large grains, carbon precipitates to several families of cementite while close to the boundaries carbon diffuses to the boundaries leaving a precipitate free zone. The formation mechanism of coalesced bainite is presented in Figure 15 along with those of upper and lower bainite.

In order to visualise the effect of Mn and Ni content on the difference between M_s and the B_s temperatures, a plot (see Figure 16) was made using the Ms and the Bs equations [34-35], as a function of Mn and Ni content along with the base input composition of 0.034 C, 0.25 Si, 0.5 Cr and 0.62 Mo (the base composition used for the neural network modelling presented elsewhere [22]). It is found that M_s and B_s are approximately equal along a line passing through the alloying content of 2 wt. % Mn and 7 wt. % Ni. It can be seen from this diagram that reducing Mn or Ni is predicted to promote bainite while increasing Mn or Ni will promote the formation of martensite. Lower M_s and B_s temperatures are found towards the upper right corner of the diagram and higher transformation temperatures towards the lower left corner. Also plotted in Figure 16 is the variation in alloying content between interdendritic and dendrite core regions as measured using EDX (Table 4) for weld metals 7-2L250 and 7-0.5L250.

The differences in microstructure across the dendrites in weld metals 7-2L250 and 7-0.5L250 may be explained in terms of the local composition measured with EDX (Table 3). Interdendritic regions which were enriched in alloying content are believed to transform at lower temperatures promoting martensite. This is supported by the greater austenite stabilisation which is also in agreement with dilatometry experiments and predictions of B_s and M_s (see Figure 16).

Finally, based on microstructural observations for the 7 wt. % Ni weld metals presented here, other nickel levels discussed elsewhere [29], dilatometry experiments, Ms and Bs predictions and literature, a constitutional diagram was constructed showing the dominant microstructural constituents as a function of nickel and manganese content. In Figure 17 microstructural regions are shown together with the martensite composition start line taken from literature [37]. Also plotted is the line where B_s and M_s are equal. In conclusion, all microstructural observations, including effects of segregation are in excellent agreement with the proposed constitutional diagram. However it should be kept in mind when applying the diagram that effects of variation in cooling rate and changes in alloying elements other than Mn and Ni also have to be considered.

4.3 Correlating properties to microstructure

A combination of 7 wt. % Ni and 2 wt. % Mn gave poor toughness but good strength. From microstructural

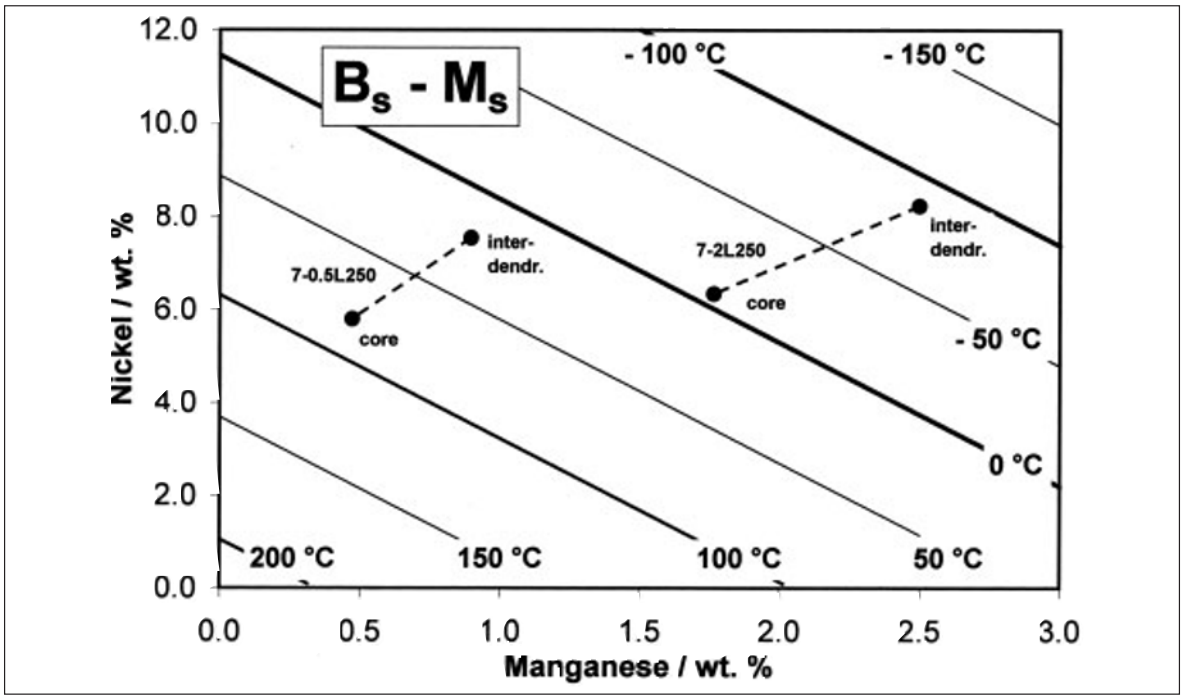

A negative difference means martensite is more likely to form while a positive value means bainite is more likely to form. The compositional variations between interdendritic and dendrite core regions are illustrated for 7-0.5L250 and 7-2L250.

Figure 16 – The difference between B_s and M_s as a function of Mn and Ni content calculated using the B_s and M_s empirical equations [34-35] along with the base input composition of 0.034 C, 0.25 Si, 0.5 Cr and 0.62 Mo

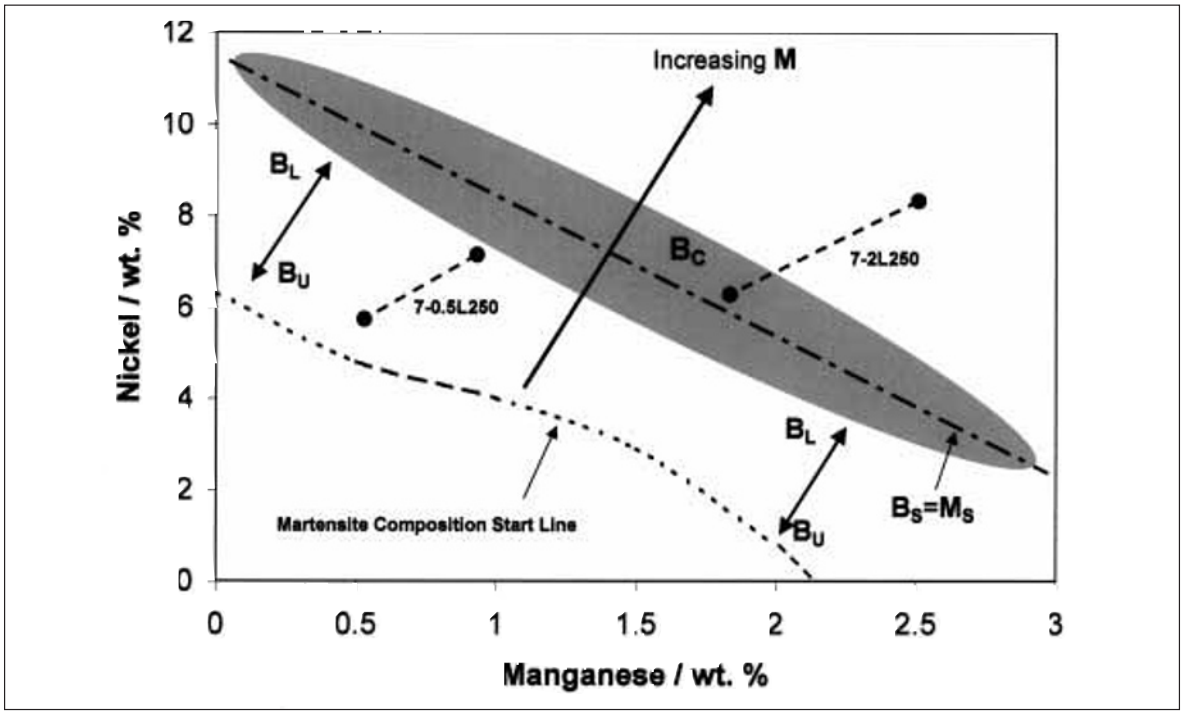

The martensite composition start line is taken from literature [37]. Also shown is the line where B_s and M_s are calculated to be equal using empirical equations [34-35].

Figure 17 – Constitutional diagram showing the dominant microstructure as a function of Ni and Mn content for the base composition 0.034 C, 0.25 Si, 0.5 Cr and 0.62 Mo

examinations, a combination of upper bainite and coalesced bainite with a very large grain size formed in dendrite core regions with martensite present at interdendritic regions. Impact toughness was most sensitive to Mn content with a dramatic increase obtained when Mn was reduced from 2 to 0.5 wt. % (see Table 2). It was found that weld metal 7-0.5L250 had the highest impact toughness but the lowest yield strength (721 MPa) and tensile strength (824 MPa) of the weld metals tested. Reducing Mn content was found to promote austenite transformation at higher temperatures with more upper and lower bainite forming. Decreasing the interpass temperature to 200 °C was found to reduce toughness marginally which was attributed to greater amounts of martensite.

Increasing carbon caused yield and tensile strength to increase while impact toughness was maintained reasonably well (see Table 2). Austenite was stabilised to lower transformation temperatures with an increasingly finer microstructure forming and martensite becoming the dominating constituent.

The amount of tempering which is largely controlled by Ac_1 and Ac_3 also has an effect on the mechanical properties in reheated regions of these weld metals. Both 7-0.5L250 and 7-0.5H200 had relatively high Ac_1 and Ac_3 values while weld metal 7-2L250 had lower Ac_1 and Ac_3 temperatures (see Table 4). As a result, with weld metal 7-2L250, less tempering takes place in regions reheated to below Ac_1 due to slower kinetics at lower temperatures and the formation of fresh untempered microstructural constituents are more likely.

It may be concluded that coalesced bainite with a large grain size is obviously unfavourable and is believed to contribute to lower yield strength and impact toughness. When combined with upper bainite and significant amounts of martensite it results in relatively high yield strength and a very high tensile strength (7-2L250) but most significantly poor impact toughness was recorded. A mixture of mainly upper and lower bainite (7-0.5L200) gave lower yield and tensile strengths with a smaller difference between the two values. For this combination of microstructural constituents very good impact toughness was recorded. A mainly martensitic microstructure (7-0.5H200) gave high yield strength and tensile strength with a small difference between the two. In addition acceptable impact toughness was recorded.

Designing high strength steel weld metals that have a combination of both high yield strength and good impact toughness is a complex task. In terms of microstructural constituents it is clear from this study and literature that interesting properties can be obtained with different proportions of upper and lower bainite along with martensite. However, compositional regions where the bainite and martensite start temperatures are close, promoting coarse grained, relatively weak and less tough coalesced bainite should be avoided. More extensive discussions on the effects of microstructure on strength and impact toughness can be found elsewhere [22].

5 CONCLUSIONS

Based on neural network modelling, experimental welds were produced using SMAW with nickel at 7 wt. % and Mn at 0.5 or 2.0 wt. %. Additional welds were made where carbon was varied between 0.03 and 0.11 wt. % with Mn set at 0.5 wt. %.

It was concluded from Thermo-Calc modelling and observed segregation behaviour that the weld metals solidified as austenite. Manganese reductions promote the decomposition of austenite at higher temperatures while carbon additions were found to stabilise austenite to lower transformation temperatures.

High manganese in combination with 7 wt. % Ni was positive for strength but very negative for toughness. Poor toughness was attributed to the presence of large grains of coalesced bainite and relatively low Ac_1 and Ac_3 temperatures which prevent effective tempering within the welded joint.

Manganese reductions lead to large increases in impact toughness. With 0.6 wt. % Mn and 6.6 wt. % Ni, 112 J at -40 °C was recorded along with a yield strength of 721 MPa. Impact toughness gain was explained by the replacement of coalesced bainite with upper and lower bainite along with greater amounts of tempering due to higher Ac_1 and Ac_3 temperatures.

Carbon additions up to 0.11 wt. % increased yield strength to 912 MPa while still maintaining toughness at over 60 J at -100 °C. Carbon additions were found to promote a fine martensitic microstructure increasing strength with limited loss of toughness.

Mechanical properties of the weld metals were explainable in terms of their relative amounts of the different microstructural constituents. Martensite was found to provide high strength and reasonable toughness whereas upper and lower bainite contributed to very good toughness and somewhat lower strength. The coarse-grained coalesced bainite found for compositions with Ms and Bs close to each other was concluded to be negative for impact toughness.

ACKNOWLEDGEMENTS

Dr. L. Karlsson of ESAB AB, Prof. H.-O. Andrén, Adjunct Prof. L.-E. Svensson of Chalmers University of Technology and Prof. H. Bhadeshia of the University of Cambridge are thanked for fruitful discussions. ESAB AB is thanked for the production of experimental weld metals, permission to publish results and financial support. The Knowledge Foundation of Sweden is thanked for additional financial support.

REFERENCES

[1] Svensson L.E.: Svetsaren, 54, January 1999.

[2] Widgery D.J., Karlsson L., Murugananth M., Keehan E.: Approaches to the development of high strength weld metals, Proceedings 2nd Int. Symposium on High Strength Steel, Norway 2002.

[3] Deloach J.F.: Proceedings, International Conference on Welding Technology, Material and Fracture, Geesthacht, Germany, 1990, F-93460 Gournay-sur-Marne, France, IITT International.

[4] Oldland P.R., Ramsay C.W., Matlock D.K., Olson D.L.: Welding Journal, April 1989, 68, p. 158.

[5] Vassilaros M.G., Czyryca E.J.: Proceedings, Advances in Low-Carbon High Strength Ferrous Alloys (LCFA-92), Jamshedpur (India), March 25-28, 1992, Key Engineering Materials (Switzerland).

[6] Fleming D.B., Bracarense A.Q., Liu S., Olson D.L.: Welding Journal, June 1996, 75, pp. 171s-183s.

[7] McRobie D.E., Knott J.F.: Material Science and Technology, May 1985, 1, pp. 357-365.

[8] Svensson L.E., Gretoft B.: Welding Journal, December 1990, 69, p. 454.

[9] Lau T.W., Sadowsky M.M., North T.H., Weaterly G.C.: The Metallurgical Society / AIME, 1987, p. 349.

[10] Lord M.: Design and modelling of ultra - High strength steel weld deposits, in materials science and metallurgy, Ph. D. thesis, University of Cambridge, UK, 1999.

[11] Abson D.J., Pargeter R.J.: Inter. Metal Rev., 1986, 31, pp. 141-194.

[12] Grong O., Matlock D.K.: Inter. Metal Rev., 1986, 31, pp. 27-48.

[13] Farrar R.A., Harrison P.L.: J. Mater. Sci., 1987, 22, pp. 239-244.

[14] Taylor D.S., Evans G.M.: Metal Constr., 1983, 15, pp. 438-443.

[15] Evans G.M.: Joining Sciences, 1991, 1, pp. 2-13.

[16] Harrison P.L., Farrar R.A.: Metal Constr., 1987, 19, pp. 392R-399R and 447R-450R.

[17] Wang W., Liu S.: Welding Journal, July 2002, p. s-132.

[18] Liao J., Kametani H., Okada H., Ikeuchi K.: Toughness of weld metals of 950 MPa high strength steel, Proceedings of the 7th Int. Symposium., 2001, pp. 809-814, Japan Welding Society.

[19] Kang Y., Kim H.J., Hwang S.K.: ISIJ International (Japan), December 2000, 40, p. 1237.

[20] Fairchild D.P., Macia M.L., Bangaru N.V., Koo J.Y.: Proc. 13th Int. Offshore and Polar Eng. Conf., Honolulu, Hawaii, USA, May 25-30 2003, p. 26.

[21] Lord M., Jennings G.: Effect of interpass temperature on properties of high strength weld metals, Svetsaren, 1999, vol. 54, no. 1-2, pp. 53-58.

[22] Keehan E., Karlsson L., Andrén H.O., Svensson L.E.: New developments with C-Mn-Ni high strength steel weld metals – Part A. Microstructure, (Keehan E., Effect of microstructure on mechanical properties of high strength steel weld metals, Ph. D. thesis, Paper 7, Chalmers University of Technology, 2004), In Manuscript.

[23] Mackay D.J.C.: Neural Computation, 1992, p. 448.

[24] Mackay D.J.C.: Neural Computation, 1992, p. 415.

[25] Bhadeshia H.K.D.H.: ISIJ International (Japan), October 1999, 39, p. 966-979.

[26] Keehan E.: Effect of microstructure on mechanical properties of high strength steel weld metals, Ph. D. thesis, Chalmers University of Technology, 2004.

[27] Keehan E., Karlsson L., Andrén H.O., Svensson L.E.: New developments with C-Mn-Ni high strength steel weld metals – Part B. Mechanical Properties, (Keehan E., Effect of microstructure on mechanical properties of high strength steel weld metals, Ph. D. thesis, Paper 8, Chalmers University of Technology, 2004), In Manuscript.

[28] Keehan E., Bhadeshia H.K.D.H., Andrén H.O., Karlsson L., Svensson L.E.: Microstructure characterisation of a high strength steel weld metal containing the novel constituent coalesced bainite, (Keehan E., Effect of microstructure on mechanical properties of high strength steel weld metals, Ph. D. thesis, Paper 3, Chalmers University of Technology, 2004), In manuscript.

[29] Keehan E., Karlsson L., Andrén H.O.: Influence of C, Mn and Ni contents on microstructure and properties of strong steel weld metals, Part I. Effect of nickel content, (Keehan E., Effect of microstructure on mechanical properties of high strength steel weld metals, Ph. D. thesis, Paper 4, Chalmers University of Technology, 2004), accepted for publication in The Science and Technology of Welding and Joining.

[30] Keehan E., Karlsson L., Andrén H.O., Bhadeshia H.K.D.H: Influence of C, Mn and Ni contents on microstructure and properties of strong steel weld metals, Part II, Impact toughness gain from manganese reductions, (Keehan E., Effect of microstructure on mechanical properties of high strength steel weld metals, Ph. D. thesis, Paper 5, Chalmers University of Technology, 2004), accepted for publication in The Science and Technology of Welding and Joining.

[31] Keehan E., Karlsson L., Andrén H.O., Bhadeshia H.K.D.H.: Influence of C, Mn and Ni contents on microstructure and properties of strong steel weld metals, Part III. Increased strength from carbon additions, (Keehan E., Effect of microstructure on mechanical properties of high strength steel weld metals, Ph. D. thesis, Paper 6, Chalmers University of Technology, 2004), accepted for publication in The Science and Technology of Welding and Joining.

[32] SSAB Oxelösund, WeldCalc, Version 1.0.0, 98 – 99R.W.K.

[33] Sundman B., Jansson B., Andersson J.O.: Calphad, 1985, vol. 9, no. 2, pp. 153-190.

[34] Honeycombe R.W.K., Bhadeshia H.K.D.K.: Steel Microstructure and Properties, 2nd Ed., 1995, Edward Arnold, London, p 103.

[35] Honeycombe R.W.K., Bhadeshia H.K.D.K.: Steel Microstructure and Properties, 2nd Ed., 1995, Edward Arnold, London, p 133.

[36] Takahashi M., Bhadeshia H.K.D.H.: Materials Science and Technology, 1990, 6, pp. 592-603.

[37] Z. Zhang, R.A. Farrar: Influence of Mn and Ni on the microstructure and toughness of C-Mn-Ni weld metals, Welding Journal, May 1997, 76, pp. S183-S196.